*Sound & Vibration* 2025, 60(3), 4136.
doi: https://doi.org/10.59400/sv4136

Article

# Bifurcation and chaos analysis of gear-bearing system with fractal mesh stiffness and fractal friction excitation

**Wei Liu[1,2], Ying Cui[1], Qiang Wang[1,*]**

[1] College of Automobile and Traffic Engineering, Heilongjiang Institute of Technology, Harbin 150050, China
[2] College of Mechanical and Electrical Engineering, Northeast Forestry University, Harbin 150040, China
*** Corresponding author:** Qiang Wang, wangqiang@hljit.edu.cn

**CITATION**

Liu W, Cui Y, Wang Q. Bifurcation and chaos analysis of gear-bearing system with fractal mesh stiffness and fractal friction excitation. Sound & Vibration. 2026; 60(3): 4136. https://doi.org/10.59400/sv4136

**ARTICLE INFO**

Received: 9 March 2026
Revised: 15 April 2026
Accepted: 20 April 2026
Available online: 25 May 2026



**Abstract:** Studying tooth surface topography and sliding friction in gear-bearing system is crucial for enhancing its reliability and minimizing vibration and noise. Inspired by preliminary research on sliding friction, this study addresses a novel gear-bearing model, in which the fractal meshing stiffness and fractal friction excitation are emphasized simultaneously. Initially, the formula of time-varying meshing stiffness (TVMS) due to fractal characterization is developed by employing the W-M function. The influence of fractal dimension on TVMS is investigated. Subsequently, the sliding friction excitation corresponding to fractal dimension is derived and introduced into the proposed gear-bearing model. On this basis, the bifurcation and chaos of the gear-bearing system with and without fractal dimension are compared. The maximum Lyapunov exponent forecasting methodology is carried out to validate the dynamic characteristics. In order to clearly exhibit the influence of the fractal dimension, the nonlinear dynamic behaviors of the gear-bearing system are investigated by reference to its time-domain chart, phase diagram, frequency spectrum, and Poincare section. Ultimately, contributions of sliding friction on dynamic behaviors of gear-bearing system are also examined. This work is extremely significant for improving the gear dynamic performance through guiding gear surface design and manufacture.

**Keywords:** gear dynamic; fractal dimension; bifurcation and chaos; TVMS (time varying meshing stiffness); sliding friction

## 1. Introduction

Noise and vibration generated by the gear system is one of the crucial factors affecting the dynamic performance and efficiency in many power transmission fields [1–4]. Owing to the increasingly requirement of reducing noise and vibration [5, 6], the quality and precision of machining of gear surface has attracted extensive attention. In this manuscript, we primarily concentrate on the systematic dynamic analysis of gear-bearing dynamic model with fractal meshing stiffness and fractal friction excitation.

In recent years, the effect of fractal characterization on the dynamic behaviors of gear-bearing systems has gradually been the focus of research. Huang et al. [7] studied the nonlinear dynamic behaviors of the spur gear pair system with fractal gear backlash, and their results show that compared with the fixed backlash case, the system with fractal backlash will be easily enter the chaotic state at a higher rotational speed. Based on fractal theory, Wang et al. [8] developed a modified multi-clearance gear system and studied the influence of bearing clearance and tooth side clearance on the nonlinear dynamic behaviors. Their research shows that while tooth side backlash and bearing backlash are considered as constants, the periodicity of the dynamic model is

essentially unchanged despite variations in clearance values. Chen et al. [9] evaluated the gears' dynamic performance influenced by gear backlash based on fractal theory. They also analyzed the influence of fractal dimension of surface morphology on gear dynamics. Huang et al. [10] investigated the influence of surface roughness on the dynamic response by introducing the fractal theory into the static transmission error. Majumdar and Bhushan [11] theoretically and experimentally demonstrated that a variety of rough surfaces are fractal in structure within millimeter scales and nanoscales. Chen et al. [12] established a modified geared rotor-bearing nonlinear dynamic model to explore the influence of microscopic features on the tooth surface based on fractal theory. Han et al. [13] examined the nonlinear dynamic behaviors of gear transmission systems through considering the tooth surface microtopography factor. Mo et al. [14] proposed an improved nonlinear dynamic model and concentrated on the influence of sliding friction and fractal roughness on the nonlinear behaviors. Yu et al. [15] addressed a novel gear fractal backlash model with joint action and validated the proposed gear model by utilizing experimental data. Wu et al. [16] experimentally investigated the influence law of tooth surface micromorphology on time-varying mesh stiffness and fault gear dynamics. Xiong et al. [17] optimized the tangential contact damping model with the fractal dimension and variable friction coefficient. Zhu et al. [18] established an improved dynamic model of helical gear pair considering distinctions in the tooth surface contact coefficients for different slices simultaneously. The effect of tooth surface morphology on the time varying mesh stiffness of helical gear pairs was analyzed. Their results show that TVMS escalates with an increase in fractal dimension and a decrease in the characteristic scale coefficient. Sun and Xin [19] proposed a fractal model of thermal contact conductance (TCC) of the involute arc cylindrical gear considering friction coefficient. The influences of fractal dimension, fractal roughness and surface modification coefficient on the TCC of the rough surface were investigated. Their results show that increasing the fractal dimension or reducing the fractal roughness enhances the TCC of the rough surface, and raising the surface correction coefficient contributes to this improvement. Guo et al. [20] established the geometric structure of involute beveloid gears through adopting the Hertz formula. The Hertz contact model and fractal contact model for involute beveloid gears were explored using fractal theory, and the distribution law of contact stress was obtained. The finite element method demonstrates that the Hertz contact stress calculation formula and fractal contact model for involute beveloid gears have high accuracy. Xu et al. [21] presented a three-dimensional fractal function model to characterize fractal characteristic of microscopic morphology of the meshing surface. They also examined how fractal characteristics of microscopic morphology of the meshing surface influence the oil film pressure, oil film thickness, oil film temperature, and contact stiffness within the helical gear meshing surface. Cai et al. [22] proposed a novel dynamic differential equation for spiral bevel gears considering the surface roughness. The vibration velocity and acceleration of spiral bevel gears with different surface roughness were revealed by combining the time-varying mesh stiffness with the dynamic equation. Additionally, the comprehensive dynamic parameter model was proposed to capture the influence of microtopological changes on gear dynamics.

In the matter of modeling the internal dynamic excitations, numerous investigations have been conducted on the dynamic behaviors of gear systems with friction excitation. Chen et al. [23] explored the nonlinear dynamics of a multi-degree gear system with dynamic backlash and friction excitations. Howard et al. [24] investigated the effect of friction on the gear system by comparing the response results with friction and without friction. Saxena et al. [25] established the dynamic model of gear system with misalignment and friction excitation. Also, they considered the effect of shaft misalignment and friction force on time-varying mesh stiffness of spur gear pair. Liu et al. [26] proposed a new rigid-flexible coupled planetary gear-bearing-rotor dynamic model including tooth surface lubrication friction and roughness. They derived the improved friction coefficient and the meshing stiffness with lubrication friction based on elastohydrodynamic lubrication theory. Additionally, they investigated the modulation influence of planetary carrier's rotational frequency and friction under different lubrication states on the dynamic response. Wang et al. [27] conducted a study in which they combined bifurcation, chaos, and largest Lyapunov exponents of gear system to capture the influence of sliding friction on the dynamic behaviors. He et al. [28] developed a novel analytical model to predict the time and frequency domain results considering friction coefficient. Zhang et al. [29] proposed a prediction method including friction-wear coupling to capture the dynamic responses of gear systems. Wang and Zhu [30] carried out dynamic analysis for the GTF gear system and achieved bifurcation and chaos behaviors under friction. Liang et al. [31] theoretically evaluated the time-varying mesh stiffness of a planetary gear set using the potential energy method. Liu et al. [32] developed a novel planetary gear model including tooth surface roughness and elastohydrodynamic lubrication. Adopting the loaded tooth contact analysis (3D-LTCA) method, they examined the coupling effect of tooth surface roughness and lubrication on meshing characteristics of planetary gears. The results show that compared with roughness, speed, and viscosity, the meshing characteristics of planetary gears are most sensitive to torque. Zheng et al. [33] proposed an improved analytical model for mesh stiffness of helical gears considering the relationship of friction and flash temperature under steady temperature field. Through comparing with the finite element result, the helical gear model was validated, and the influence of friction coefficient, bulk temperature, and gear parameters on TVMS was also investigated. Xiao et al. [34] developed a new tribological model of micro-textured gear tooth in elastohydrodynamic lubrication (EHL) contact considering the coupled effect of rough surface topography. They investigated and discussed the effects of surface roughness and micro-texture parameters on the lubrication behavior, friction coefficient, and fatigue life. Also, experimental validation was performed and good agreement was obtained between the model predictions and experimental results. Li and Kahraman [35] developed a novel model to predict load-dependent (mechanical) power losses of spur gear pairs based on the elastohydrodynamic lubrication (EHL) model. Correction factors were introduced for the power losses to account for the thermal effects. They assessed the accuracy of the proposed model through comparisons to published spur gear efficiency experiments. Luo et al. [36] provided an improved analytical model to calculate the mesh stiffness

of the planetary gear set with sliding friction through considering the tooth profile beginning with the root circle. Their results show that the improved analytical model can increase the precision of the TVMS. Besides, the effect of sliding friction and spalling defects on the TVMS is significant.

To the authors' knowledge, although scholars have conducted numerous works on the nonlinear dynamics of gear-bearing models, there is still little study on the comprehensive gear-bearing model coupled with fractal meshing stiffness and fractal friction excitation. Moreover, unlike the majority of literature published by introducing fractal characterization into the gear backlash equation, in this work, the fractal meshing stiffness is modeled utilizing potential energy method. Inspired by our preliminary research on sliding friction [37–39], this work aims to expand the previous study by incorporating the fractal sliding friction into the dynamic model to guarantee the exactitude of the mapping relationship based on fractal theory. Therefore, one main objective of this work is to develop a novel gear-bearing model to exhibit nonlinear dynamic behaviors caused by fractal dimension and sliding friction [40].

This work is summarized as follows. In Section 2, the meshing stiffness with fractal characterization is considered based on fractal theory. The fractal expression related to the W-M function is developed. Height of surface morphology with two-dimensional and three-dimensional fractal W-M function is presented. In Section 3, the curvature radius, relative sliding velocity, and friction coefficient are presented to study the gear meshing characteristic. The expressions of friction coefficient and meshing force considering fractal characterization are also given. Additionally, the effect of fractal characterization on the sliding friction excitation is illustrated. In Section 4, a gear dynamic model with fractal meshing stiffness and fractal friction excitation is proposed. Meanwhile, the nonlinear dynamic model including fractal characterization is established and emphasized mathematically. In Section 5, the bifurcation diagram of the gear-bearing system with various excitation frequency with respect to fractal dimension is presented. The time-domain chart, phase diagram, frequency spectrum, and Poincare map with respect to various values of fractal dimension are presented. Additionally, the maximum Lyapunov exponent forecasting methodology is conducted to evaluate and confirm the system's stability. Bifurcation diagrams of gear system with various excitation frequency with respect to friction coefficient are compared and analyzed. In Section 6, a conclusion is given. This work is extremely valuable for the dynamic study of gear systems, especially for guiding gear surface design and improving gear dynamic performance [41–43].

## 2. Meshing stiffness with fractal characterization

### 2.1. Fractal expression of tooth surface

A meshing spur gear is presented in **Figure 1**.

Based on the well-known gear meshing theory, the expression of the involute equation can be written as:

$$\begin{cases} x_i = r_i \, cos \, (\gamma_i) \\ y_i = r_i \, sin \, (\gamma_i), \end{cases} \tag{1}$$

where the angle is $\gamma_i = s/(2r) - (inv\alpha_i - inv\alpha_0)$. $s$, $r$, $\alpha_0$ are the tooth thickness, radius and pressure angle of pitch circle. $\alpha_i$ is the pressure angle corresponding to a random position on the involute tooth profile.

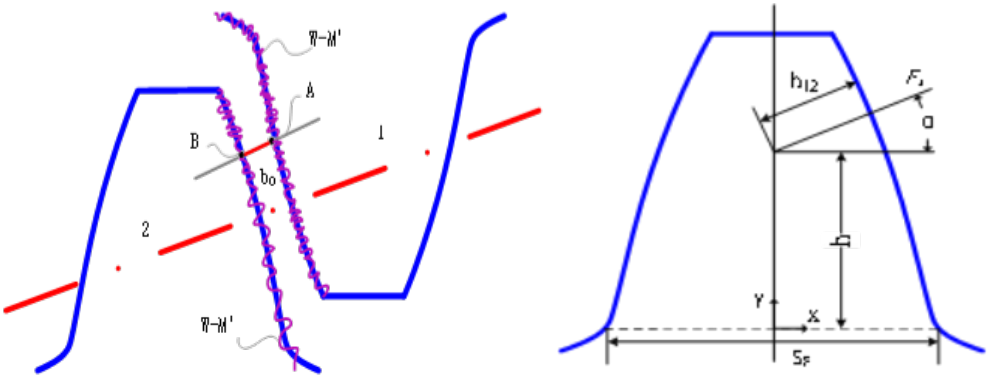


**Figure 1.** Sketch map of tooth surface morphology.

For the matching gears, the tooth surface is generally regarded as a smooth morphology, and this assumption has been applied to analyze the meshing characteristics of gear pairs by a great variety of representative literature [1,8,20,21,28]. Actually, due to the existence of practically microscopic features figuratively described in **Figure 1**, the tooth surface is affected by the surface roughness and fractal dimension. The fractal characteristics of rough surfaces can be simulated and generated by employing the W-M function. The asperity height of the two-dimensional gear surface morphology can be mathematically described, and the corresponding mathematical formula is proposed as [7]:

$$Z(x) = L(\frac{G}{L})^{D-1} \sum_{n=0}^{\infty} \gamma^{-(2-D)n} \, cos\,((2\pi\gamma^n x)/L), 1 < \mathrm{D} < 2, \gamma > 1, \quad (2)$$

where $Z(x)$ represents the random asperity height of the rough surface. $G$ is the characteristic-scale coefficient. $D$ is the fractal dimension. $\gamma^n$ is the discrete frequency spectrum. $L$ is the sampling length. $x$ is the position coordinates.

The characteristic analysis and fractal characterization of three-dimensional surface morphology is extremely crucial in understanding the dynamic performance of gear transmission. In order to better describe the fractal characteristics of surface morphology, the three-dimensional fractal expression related to the W-M function can be further developed as:

$$Z(x,y) = L(\frac{G}{L})^{D-2}(\frac{ln\gamma}{M})^{1/2} \sum_{M}^{m=1} \sum_{n_{\max}}^{n=0} \gamma^{(D-3)n}\{cos\,\phi_{m,n} - cos\,[\frac{2\pi\gamma^n(x^2+y^2)^{1/2}}{L} cos\,(arctan\frac{y}{x} - \frac{\pi m}{M}) + \phi_{m,n}]\}. \quad (3)$$

The tooth surface is curved, and the surface morphology of machined gear has an evident fractal characteristic. According to Equations (1) and (2), the meshing characteristics and dynamic performance of the rotating gear are easily affected by the tooth surface morphology. Accordingly, the expression of the involute equation including fractal surface morphology can be rewritten as:

$$\begin{cases} x_i = r_i \, cos\,(\gamma_i) \\ y_i = r_i \, sin\,(\gamma_i) + Z(x). \end{cases} \quad (4)$$

In order to reveal the physical significance of fractal dimension $D$ on the surface morphology, the asperity height curves for the two-dimensional gear surface morphology can be depicted evidently by employing the W-M function, i.e., Equation (2). It can be observed from **Figure 2** that with the value of fractal dimension increase, the amplitude of the surface morphology height decreases gradually. In other words, the surface morphology becomes refined gradually. This phenomenon indicates that the W-M function can be smoothly employed to simulate and evaluate the gear surface morphology.

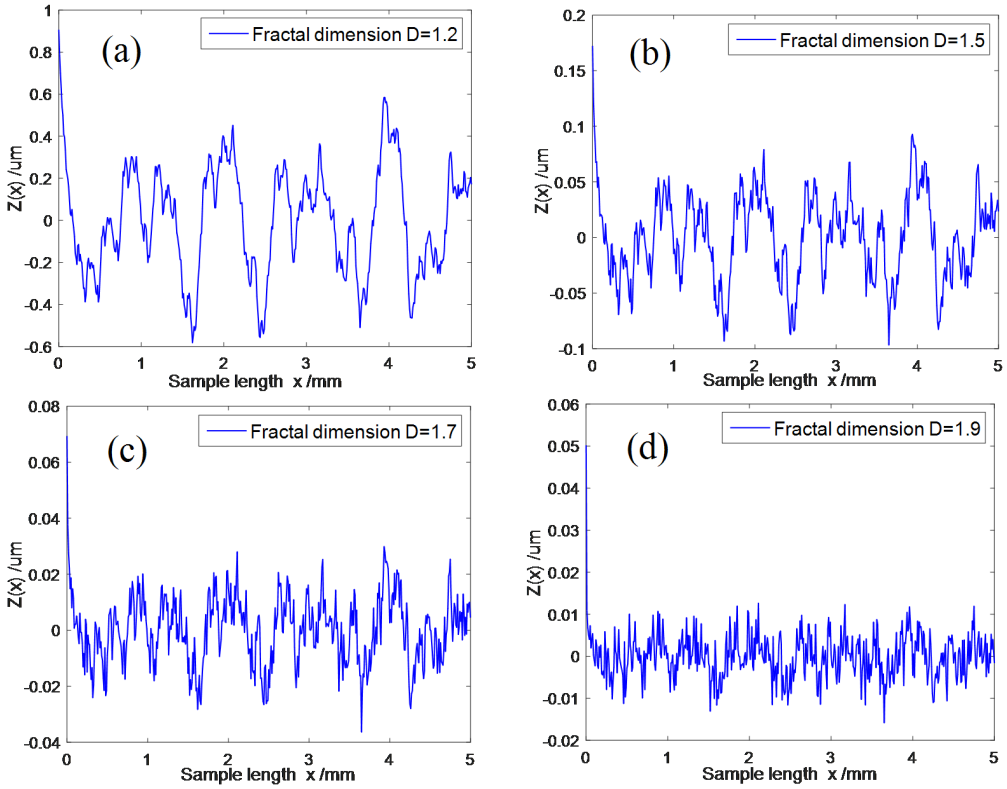


**Figure 2.** Height of surface morphology with two-dimensional fractal W-M function: **(a)** Fractal dimension $D = 1.2$; **(b)** Fractal dimension $D = 1.5$; **(c)** Fractal dimension $D = 1.7$; **(d)** Fractal dimension $D = 1.9$.

Based on the three-dimensional W-M function in Equation (3), the spatial curves of the fractal surface morphology can be plotted, as shown in **Figure 3**. Here, the fractal dimension $D = 1.7, 2.5, 2.9$ is taken as an example to illustrate the influence of fractal dimension on the surface morphology. The result indicates that with the fractal dimension increase, the surface morphology becomes refined gradually, which is consistent with the phenomenon in the two-dimensional morphology simulation.

In summary, the proposed formula for the surface morphology is beneficial and will be employed for the following fractal meshing stiffness study.

## 2.2. Expression for the Hertz stiffness, bending stiffness, axial compression stiffness, and shear stiffness including fractal characteristics

In this section, the potential energy method for a pair of external-internal gears will be employed for the purpose of obtaining the developed TVMS formula including fractal characterization of gear surface morphology. The specific derivation process can

be found and captured in He et al. [28]. Expressions of the Hertz stiffness, bending stiffness, axial compression stiffness, and shear stiffness including fractal characteristics will be re-modified. Here, the Hertz stiffness is not affected by the fractal factor and can be written as:

$$k_h = \frac{F}{\delta} = \frac{\pi EL}{4(1-\nu^2)}. \tag{5}$$

With respect to a meshing gear pair, the bending stiffness $k_b$, shear stiffness $k_s$ and axial compression stiffness $k_a$ are proposed as [28]:

$$\frac{1}{k_b} = \int_0^d \frac{[(d-x)\,cos\,a_1 - h\,sin\,a_1]^2}{EI_x} dx, \tag{6}$$

$$\frac{1}{k_s} = \int_0^d \frac{1.2\,cos^2\,a_1}{GA_x} dx, \tag{7}$$

$$\frac{1}{k_a} = \int_0^d \frac{sin^2\,a_1}{EA_x} dx, \tag{8}$$

where $I_x$ is the area moment of inertia. $E$ is the Young's modulus. $G$ is the shear modulus. $d$ is the distance between the contact point and the tooth root. $a_1$ is the angle between the component force. $A_x$ is the cross-sectional area.

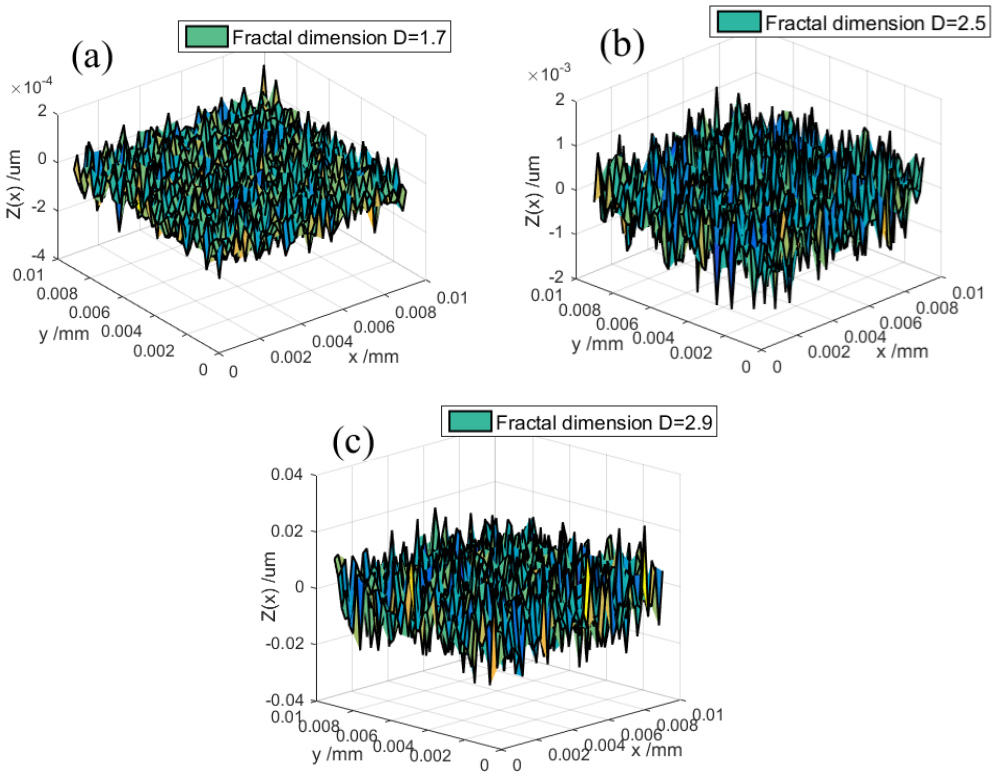


**Figure 3.** Height of surface morphology with three-dimensional fractal W-M function: **(a)** Fractal dimension $D$ = 1.7; **(b)** Fractal dimension $D$ = 2.5; **(c)** Fractal dimension $D$ = 2.9.

The fractal surface morphology can affect the meshing characteristics of gear pairs, as illustrated in Equation (4). Inspired by the involute equation in Equation (4) and tooth deformation in **Figure 4**, the shear stiffness $k_s$ and axial compression stiffness $k_a$ are unchanged. Correspondingly, the bending stiffness $k_b$ with fractal characterization can

be re-modified as:

$$\frac{1}{k_b} = \int_0^d \frac{[(d - x + \mathrm{Z}(x))\ cos\ a_1 - h\ sin\ a_1]^2}{EI_x} dx. \tag{9}$$

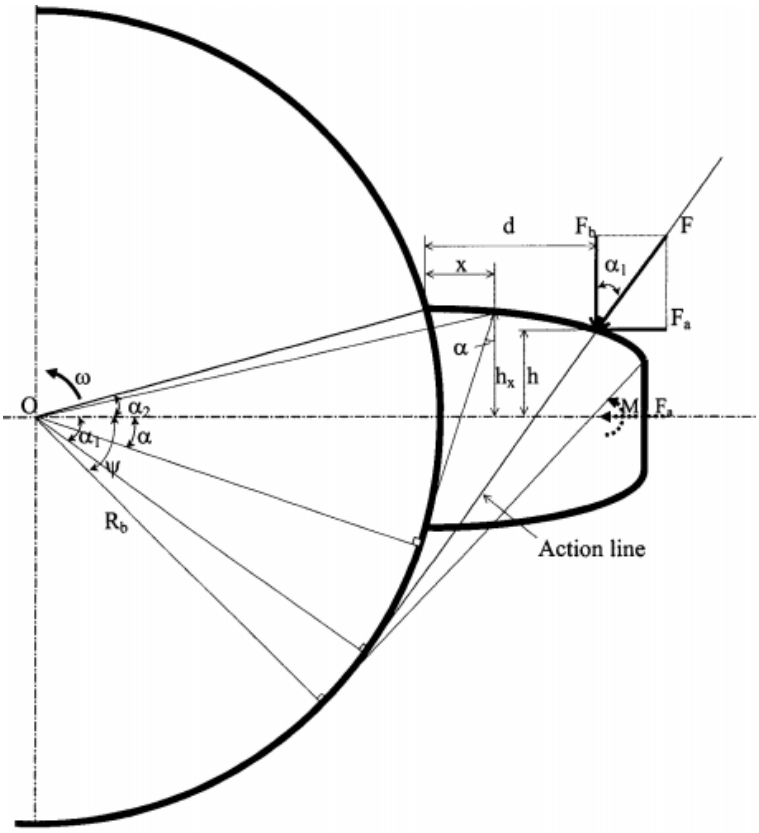


**Figure 4.** Teeth force of an internal meshing gear pair [5].

For an internal meshing gear pair (**Figure 5**), the bending stiffness with fractal characterization can be converted to:

$$\frac{1}{k_b} = \int_\phi^{\beta_1} \frac{3\{1 + cos\ \beta_1[(\beta_2 - \beta)\ sin\ \beta - cos\ \beta + Z(x)]\}^2 \times (\beta_2 - \beta)\ cos\ \beta}{2EL[sin\ \beta + (\beta_2 - \beta)\ cos\ \beta]^3} d\beta. \tag{10}$$

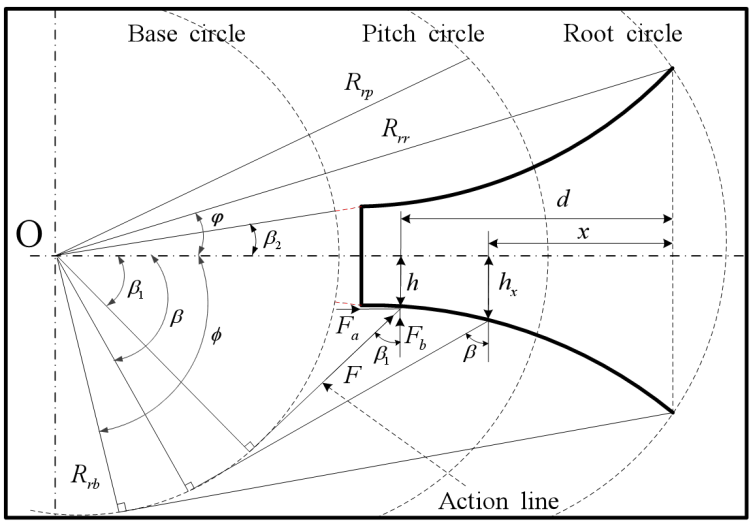


**Figure 5.** Teeth force of internal gear.

The shear stiffness is unchanged and proposed as:

$$\frac{1}{k_s} = \int_{\phi}^{\beta_1} \frac{1.2(1+\nu)\, cos^2\, \beta_1(\beta_2-\beta)\, cos\, \beta}{EL[\, sin\, \beta + (\beta_2-\beta)\, cos\, \beta]} d\beta. \tag{11}$$

The axial compression stiffness $k_a$ is unchanged and proposed as:

$$\frac{1}{k_a} = \int_{\phi}^{\beta_1} \frac{(\beta_2-\beta)\, cos\, \beta\, sin^2\, \beta_1}{2EL[\, sin\, \beta + (\beta_2-\beta)\, cos\, \beta]} d\beta, \tag{12}$$

where $\beta_2 = \pi/2N_2 - tan\ \alpha_0 + \alpha_0$ represents the half tooth angle of base circle. $\phi = \beta_2 + tan\,(arccos R_{rb}/R_{rr})$ is the half tooth angle of tooth circle. $R_{rb}$ is the base circle radius. $R_{rr}$ is the tooth root circle radius. $\beta_1$ is the angle between the component force $F_b$ and the resultant force $F$.

For an external meshing gear pair (**Figure 6**), the modified bending stiffness $k_b$, the shear stiffness $k_s$ and the axial compression stiffness $k_a$ are proposed as:

$$\frac{1}{k_b} = \int_{-\alpha_1}^{\alpha_2} \frac{3\left\{1 + cos\ \alpha_1[(\alpha_2-\alpha)\, sin\, \alpha - cos\, \alpha] + Z(x)\right\}^2 \times (\alpha_2-\alpha)\, cos\, \alpha}{2EL[sin\, \alpha + (\alpha_2-\alpha)\, cos\, \alpha]^3} d\alpha, \tag{13}$$

$$\frac{1}{k_s} = \int_{-\alpha_1}^{\alpha_2} \frac{1.2(1+\nu)\, cos^2\, \alpha_1(\alpha_2-\alpha)\, cos\, \alpha}{EL[sin\, \alpha + (\alpha_2-\alpha)\, cos\, \alpha]} d\alpha, \tag{14}$$

$$\frac{1}{k_a} = \int_{-\alpha_1}^{\alpha_2} \frac{(\alpha_2-\alpha)\, cos\, \alpha\, sin^2\, \alpha_1}{2EL[sin\, \alpha + (\alpha_2-\alpha)\, cos\, \alpha]} d\alpha, \tag{15}$$

where $\alpha_2 = \pi/2N_1 + tan\ \alpha_0 - \alpha_0$ is the half tooth angle of the base circle. $\alpha_1$ is the angle between the component force $F_b$ and the resultant force $F$. $\alpha_0$ is the pressure angle.

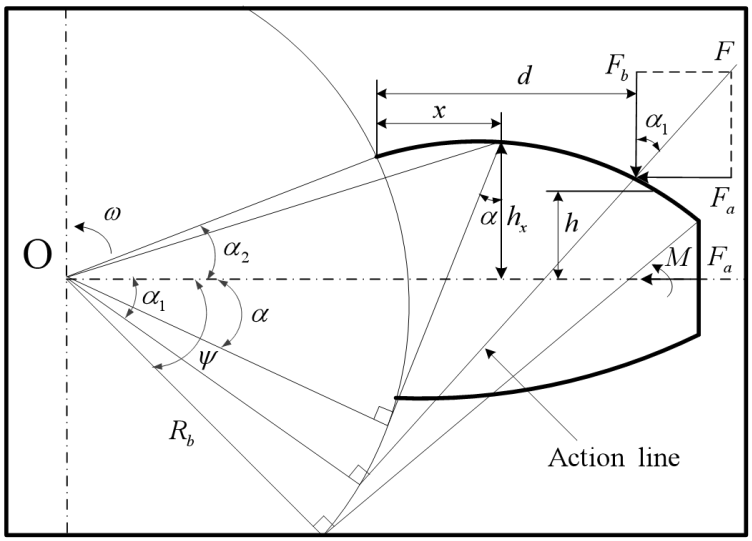


**Figure 6.** Teeth force of external gear.

Ultimately, the total effective meshing stiffness including fractal characteristics can be constructed mathematically as:

$$k_r(\theta) = \frac{1}{\frac{1}{k_h} + \frac{1}{k_{b1}} + \frac{1}{k_{s1}} + \frac{1}{k_{a1}} + \frac{1}{k_{b2}} + \frac{1}{k_{s2}} + \frac{1}{k_{a2}}}, \tag{16}$$

where $k_r(\theta)$ represents the modified meshing stiffness for single-tooth-pair mesh duration.

## 2.3. Verification

To validate the correctness of fractal meshing stiffness calculation, numerical examples on the meshing characteristics of a pair of external-internal gears are presented here through employing the potential energy method. The gear's parameters tabulated in **Table 1** are completely consistent with the data in Liang et al. [31]. The corresponding characteristic curves of TVMS considering fractal characterization for the external and internal gears are calculated theoretically, as is depicted in **Figures 7** and **8**. Simultaneously, the zoomed curves are redrawn for the purpose of better illustration of the fractal characteristic, as shown in **Figures 7b** and **8b**. It can be observed that the simulated curves are basically consistent with the published results in Liang et al. [31].

In order to further illustrate the effect of surface morphology on the TVMS, the fractal meshing stiffness curves versus the variation of fractal dimension are depicted in **Figure 9**. It can be found that after introducing the fractal parameter *D*, the TVMS curves exhibit extremely complex fluctuation behavior. With the value of fractal dimension increasing, the fractal meshing stiffness becomes not significant. Additionally, comparing with the smooth tooth surface case $D = 0$, the fluctuated fractal meshing stiffness are decreased, which is primarily caused by the various heights of the surface morphology. It can be concluded that the surface morphology with fractal characterization is a primary factor in generating the vibration response of gear pairs.

**Table 1.** Main parameters.

| Modulus (mm) | Angle | Width (m) | Young's Modulus (Pa) | Poisson's ratio | Sun teeth | Planet teeth | Ring teeth |
|---|---|---|---|---|---|---|---|
| 3.2 | 20° | 0.0381 | 2.07E+11 | 0.3 | 19 | 31 | 81 |

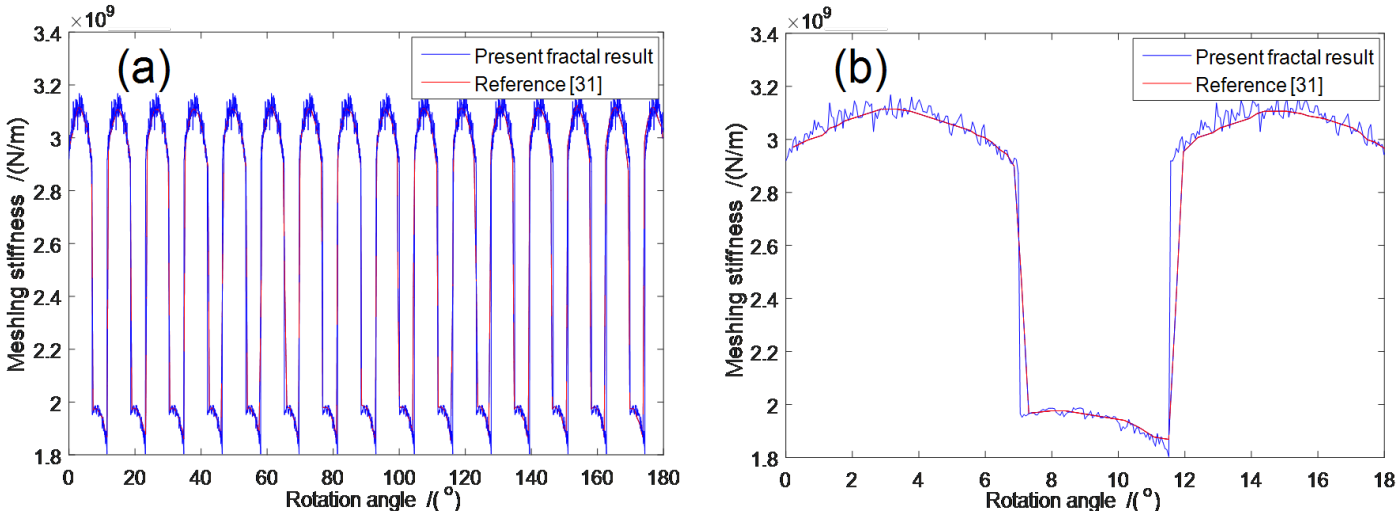


**Figure 7.** Fractal meshing stiffness for an external gear: **(a)** Integrated graph; **(b)** Zoomed graph.

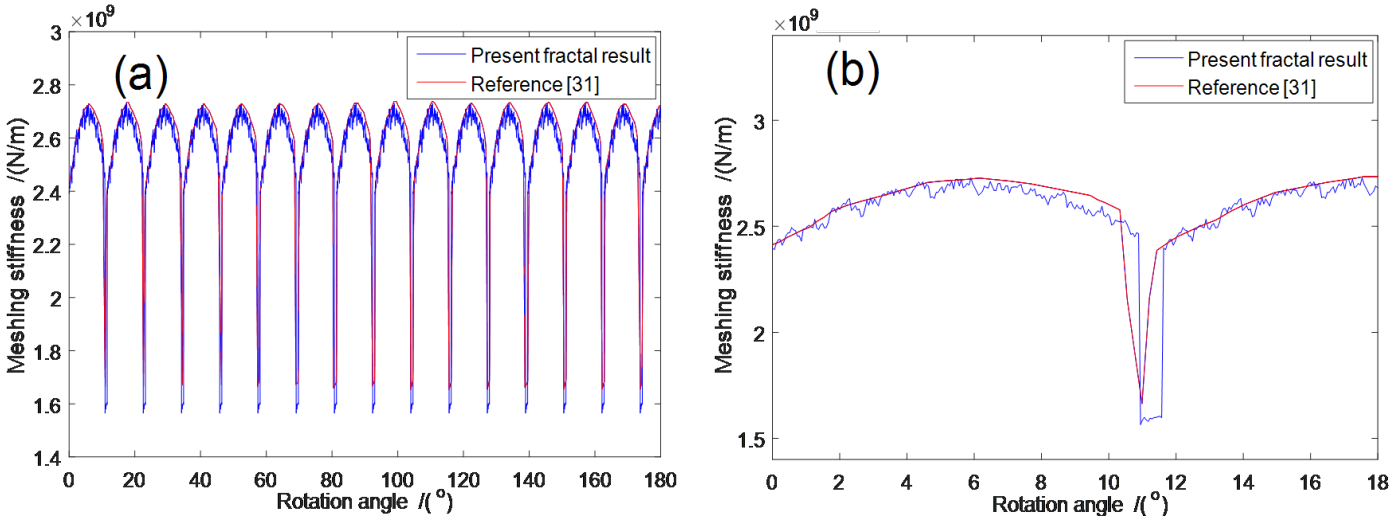


**Figure 8.** Fractal meshing stiffness for an internal gear: **(a)** Integrated graph; **(b)** Zoomed graph.

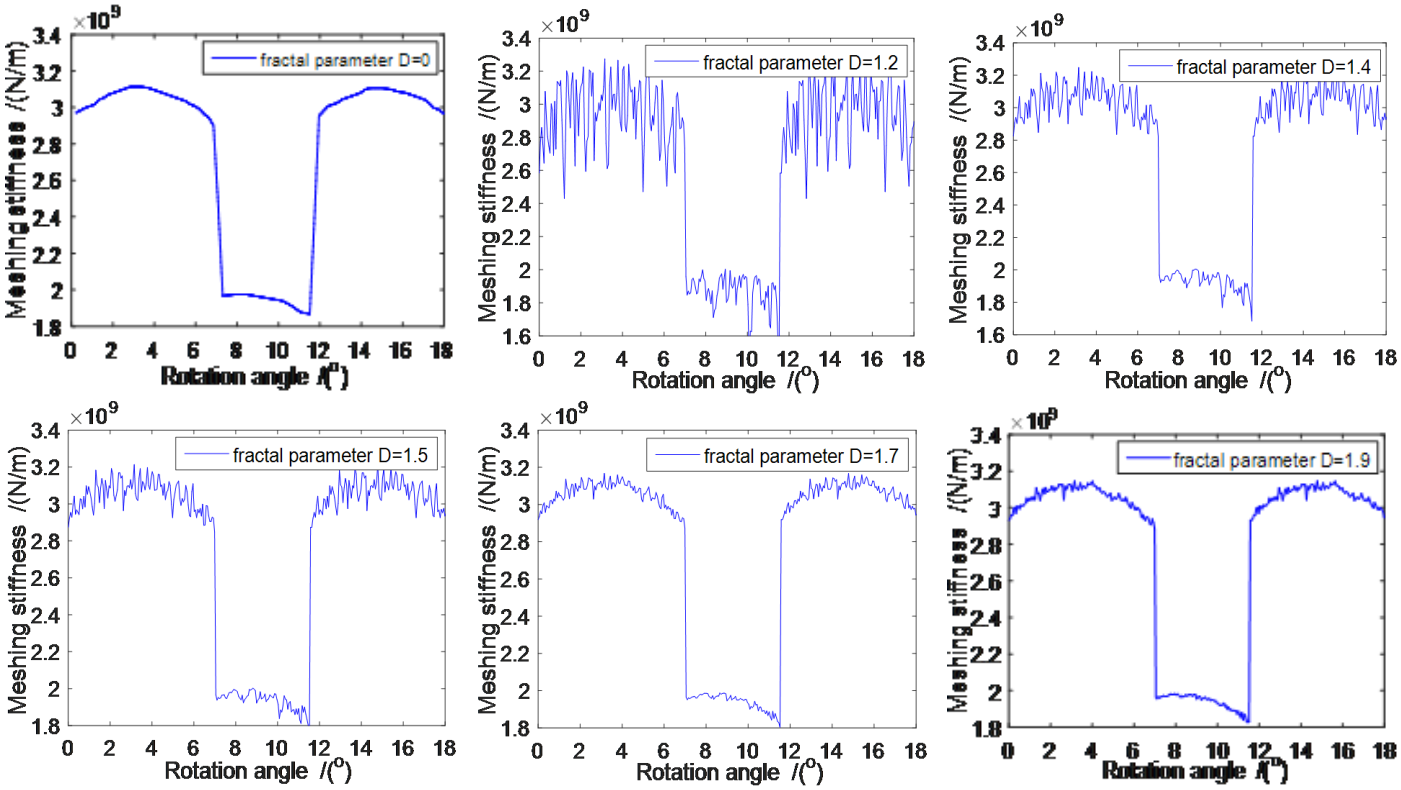


**Figure 9.** Meshing stiffness with respect to various fractal dimension parameter.

## 3. Friction excitation force with fractal characterization

In the previous study, the meshing process for the drive gear and the driven gear has been investigated in one engagement period. The curvature radius, relative sliding velocity, and friction coefficient are fundamental to deeply study the gear meshing characteristic. These introduced parameters are extremely significant and will be helpful for the analysis of the friction excitation force with fractal characterization.

For a meshing gear pair, the curvature radius and the integrated curvature radius

are proposed as [28]:

$$\begin{cases} R_1 = N_1A_1 + r_{1p} = (r_1 + r_2)\ sin\ \alpha - \sqrt{r_{a2}^2 - r_{b2}^2} + r_{1p} \\ R_2 = N_1N_2 - R_1 = \sqrt{r_{a2}^2 - r_{b2}^2} - r_{1p} \\ R_{12} = R_1R_2/(R_1 + R_2). \end{cases} \tag{17}$$

The relative sliding velocity formulas are expressed as:

$$\begin{cases} v_1 = \omega_1R_1 = 2\pi n_1[(r_1 + r_2)\ sin\ \alpha - \sqrt{r_{a2}^2 - r_{b2}^2} + r_{1p}] \\ v_2 = \omega_2R_2 = 2\pi n_2(\sqrt{r_{a2}^2 - r_{b2}^2} - r_{1p}) \\ v_{12} = v_1 - v_2. \end{cases} \tag{18}$$

The expression of friction coefficient can be written as:

$$\mu = 0.002(\frac{F_t}{b \times 0.001})^{0.2}[\frac{2000}{cos\ \alpha_t(V_{t1} + V_{t2})R_E}]^{0.2}\eta^{-0.05}X_R. \tag{19}$$

Hence, the friction excitation force can be formulated as:

$$F_f = \eta_1\mu F_{mesh} = \eta_1\mu e(t)k_r(\theta), \tag{20}$$

where $F_f$ is the friction excitation force. $\eta_1$ is the direction of friction excitation force and $\eta_1 = \pm 1$. Here, $e(t)$ is the transmission error. $k_r(\theta)$ is the TVMS.

The friction torque is deduced as follows:

$$M_f = R_fF_f = R_f\eta_1\mu F_{mesh} = R_f\eta_1\mu e(t)k_r(\theta), \tag{21}$$

where $\eta_1 = \text{sign}(Vs)$ is adopted to determine the positive or negative values.

The gear parameters tabulated in **Table 1** are employed to calculate the curvature radius, relative sliding velocity, and friction coefficient, as is depicted in **Figure 10a**. It can be found that the curvature radius of the drive gear is increasing and the curvature radius of the driven gear is decreasing gradually. They intersect at one point simultaneously. The absolute sliding velocity presents a similar phenomenon, as shown in **Figure 10b**. It can be found that the relative sliding velocity is zero at the pitch circle. The friction coefficient becomes large or small due to the change of single and double teeth intervals. **Figure 10c** indicates that the direction of the friction coefficient changes invariably, which is primarily determined by the sliding velocity, as described in Equation (19).

Additionally, the transmission error and TVMS curves are plotted in **Figure 11a,b**. According to the equation $F_{mesh} = ek_r(\theta)$, one can obtain the meshing force curve, as shown in **Figure 11c**. It can be found that the meshing force curve indicates a surface morphology, which is similar to the fractal meshing stiffness in **Figure 9**. Combining the friction coefficient formula and meshing force formula shown in Equation (20), it is easily to predict that the friction excitation force can perform the fractal characteristic. And the fractal friction excitation force will be employed to calculate the dynamic response of gear pairs.

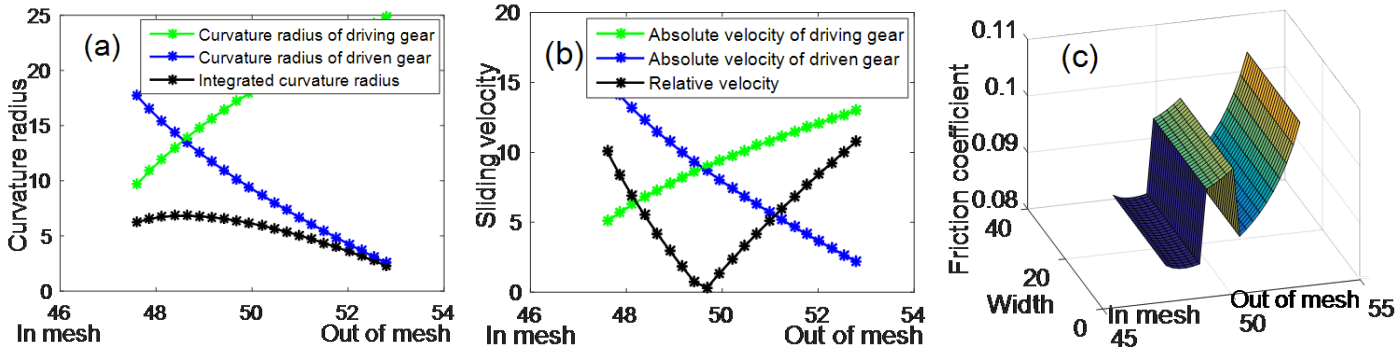


**Figure 10.** Change rule of the curvature radius, relative sliding velocity, and friction coefficient: **(a)** Curvature radius; **(b)** Absolute sliding velocity; **(c)** Friction coefficient.

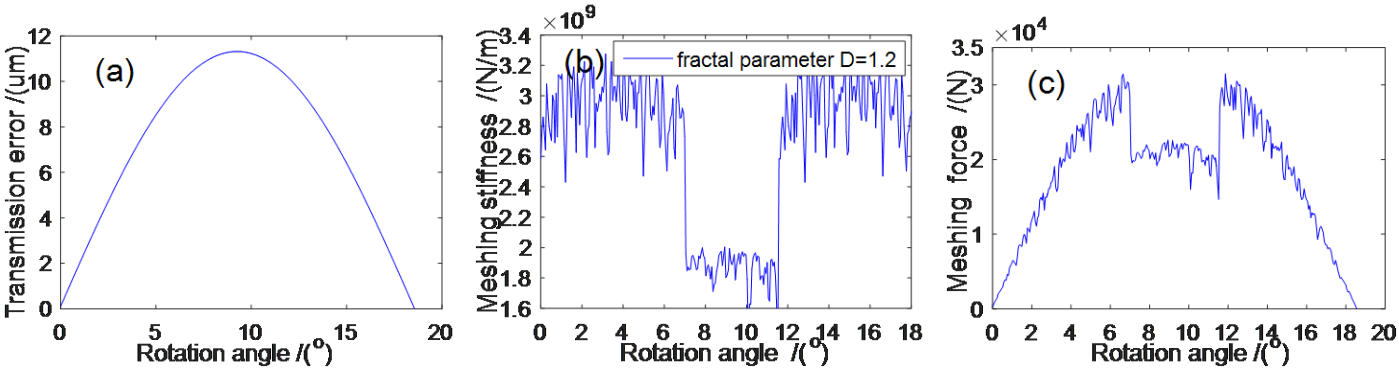


**Figure 11.** Meshing force considering fractal characterization: **(a)** The transmission error; **(b)** The TVMS curve; **(c)** The meshing force curve.

## 4. Dynamic model and governing equation

In this section, the nonlinear dynamic model of a spur gear pair including fractal characterization is established mathematically. In this model, the fractal meshing stiffness and fractal friction excitation force are emphasized simultaneously. The nonlinear dynamic model for three degrees of freedom is depicted in **Figure 12**. The governing equation coupling transverse-torsional motion for the spur gear system is proposed as [32]:

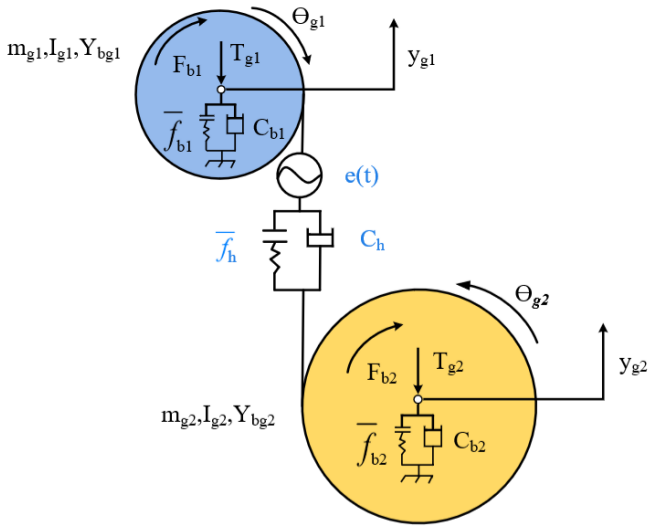


**Figure 12.** The nonlinear dynamic model of gear-bearing system.

$$\begin{cases} m_{g1}y_{g1}^{"} + c_{b1}y_{g1}' + c_h(x' + y_{g1}' - y_{g2}' - e') + k_{b1}\, f_{b1}(y_{b1}) + k_h(t)f_h(x + y_{g1} + y_{g2} - e) = -F_{b1} \\ m_{g2}y_{g2}^{"} + c_{b2}y_{g2}' - c_h(x' + y_{g1}' - y_{g2}' - e') + k_{b2}f_{b2}(y_{b2}) - k_h(t)f_h(x + y_{g1} - y_{g2} - e) = F_{b2} \\ m_{c1}x^{"} + c_h(x' + y_{g1}' - y_{g2}' - e') + k_h(t)f_h(x + y_{g1} + y_{g2} - e) = F_m + F_{aT}(t) + M_f/R_{12}, \end{cases} \tag{22}$$

where $I_{g1}$, $I_{g2}$ are the moment of inertia of the driving gear and driven gear, respectively. $m_{g1}$, $m_{g2}$ are the mass. $I_{g1}$, $I_{g2}$ are the radius of the base circle. $F_{b1}$, $F_{b2}$ are bearing force. $T_{g1}$, $T_{g2}$ are torque. $C_{b2}$, $C_{b2}$ are damping coefficient. $\theta_{g1}$, $\theta_{g2}$ are torsional angular. $\overline{f}_{b1}$, $\overline{f}_{b2}$ are displacement function (**Figure 12**). $k_{b1}$, $k_{b2}$ are bearing stiffness. $c_h$ is damping coefficient. $M_f$ is friction torque. $\overline{f}_h$ is displacement function. $y_{g1}$, $y_{g2}$ represent central displacement between driving gear and driven gear. $e(t)$ is tangential error along gear base circle. The geometric parameters of sun-planet meshing gear pairs are tabulated in **Table 1**.

The specific expression of the gear parameters can be defined as:

$$x(t) = r_{bg1}\theta_{g1}(t) - r_{bg2}\theta_{g2}(t), \tag{23}$$

$$m_{c1} = 1/\left(r_{bg1}^2/I_{g1} + r_{bg2}^2/I_{g2}\right), \tag{24}$$

$$F_m = T_{g1m}/r_{bg1} = T_{g2m}/r_{bg2,} \tag{25}$$

$$F_{aT}(t) = m_{c1}T_{g1a}(t)/(2I_{g1}), \tag{26}$$

$$k_h(t) = k_h(t + 2\pi/\Omega_h) = k_{hm} + \sum\nolimits_{r=1}^{\infty} k_{har}\, cos\, (r\Omega_h t + \phi_{hr}), \tag{27}$$

where $T_{g1a}(t)$ is variable torque value. $T_{g1m}$, $T_{g2m}$ are average value of input and output torque. $T_{g1}(t)$, $T_{g2}(t)$ are input and output torque. $k_h(t)$ represents gear meshing stiffness varying with time cycle. $k_{hm}$ is average value of meshing stiffness. $k_{har}$ is coefficient of each harmonic component. $\phi_{hr}$ is corresponding phase angle. $\Omega_h$ is meshing frequency. The relative torsional displacement of gear pair is defined as:

$$p(t) = r_{bg1}\theta_{g1}(t) - r_{bg2}\theta_{g2}(t) - y_{g1}(t) + y_{g2}(t) - e(t). \tag{28}$$

By taking $x_1 = y_{g1}, x_3 = y_{g2}, x_5 = p$, Equation (21) can be rewritten as follow:

$$\begin{cases} {x_1}' = x_2 \\ {x_2}' = -F_{b1} - 2\xi_{11}x_2 - 2\xi_{13}x_6 - k_{11}x_1 - k_{13}(t)f_h\,(x_5) \\ x_3' = x_4 \\ x_4' = F_{b2} - 2\xi_{22}x_4 + 2\xi_{23}x_6 - k_{22}x_3 + k_{23}(t)f_h\,(x_5) \\ x_5' = x_6 \\ x_6' = F_m + F_{ah1}\omega^2\cos(\omega t) + x_2' - x_4' - 2\xi_{33}x_6 - k_{33}(t)f_h\,(x_5) + M_f/R_{12} \end{cases}, \tag{29}$$

where $x_1$, $x_3$, $x_5$ are the relative torsional displacement of driving gear, driven gear, and gear transmission. $x_2$, $x_4$, $x_6$ are the corresponding speeds. The calculation formula of TVMS is $k_{33}(t) = 1 - \varepsilon\, cos\ (\Omega_h t)$ and $k_{13}(t) = k_{23}(t) = k_{33}(t)/4$, respectively. Note that TVMS $k_{33}(t)$ will be replaced with $k_r(\theta)$ proposed in Equation (16) in the following study.

The nonlinear displacement function of the meshing gear can be expressed as:

$$f_h(x_5) = \begin{cases} x_5 - B & x_5 > B \\ 0 & -B \le x_5 \le B \\ x_5 + B & x_5 < -B \end{cases}, \tag{30}$$

where $B$ is the non-dimensional backlash.

## 5. Simulation of dynamic performance based on the fractal method

In this section, the influence of key parameters in the novel gear-bearing system is evaluated based on fractal theory, particularly concentrating on the microscopic features i.e., fractal dimension and sliding friction. The nonlinear dynamic behaviors of gear-bearing system will be examined by utilizing MATLAB software.

### 5.1. Bifurcation and chaos influenced by excitation frequency

To significantly exhibit the variation of nonlinear dynamic behaviors, the bifurcation and chaos of the gear-bearing system with and without fractal dimension are compared theoretically. To make the comparison more reasonable, in this case, the friction excitation is not considered and set identically to zero. The bifurcation diagrams of gear-bearing system with various excitation frequency $w_m$ with respect to fractal dimension $D = 0$ and $D = 1.2$ are presented figuratively, as shown in **Figure 13**.

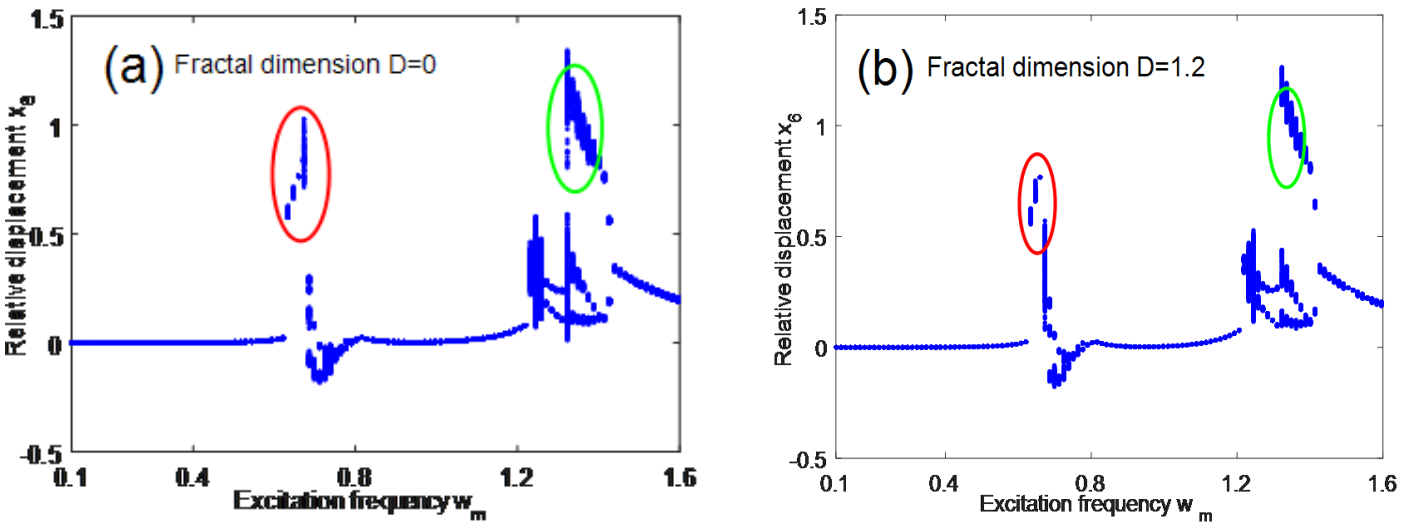


**Figure 13.** Bifurcation diagram of gear-bearing system with various excitation frequency $w_m$ with respect to fractal dimension: **(a)** $D = 0$; **(b)** $D = 1.2$.

In comparison with not considering fractal dimension case, the newly emerging chaotic motion of gear-bearing system presented in **Figure 13b** is greatly weakened and the relative displacement becomes smaller. These variations can be clearly observed in the green area in **Figure 13**. Similarly, while the fractal dimension $D = 1.2$ is introduced, the relative displacement tends to decrease accordingly, as described in the red area. Actually, the reduction of displacement amplitude is primarily caused by the smaller value of TVMS corresponding to fractal dimension $D = 1.2$, which has been demonstrated and elaborated in **Figure 9** in Subsection 2.3. Additionally, adopting the

Jacobian approach, maximum Lyapunov exponent forecasting methodology is conducted to evaluate and confirm the system's stability. It is extensively recognized that the negative and positive maximum Lyapunov exponents below and above the red line in **Figure 14** are regarded as the periodic motion and chaotic state, respectively. The predicted maximum Lyapunov exponent result is completely consistent with those in **Figure 13b**, which validates the system's nonlinear behaviors.

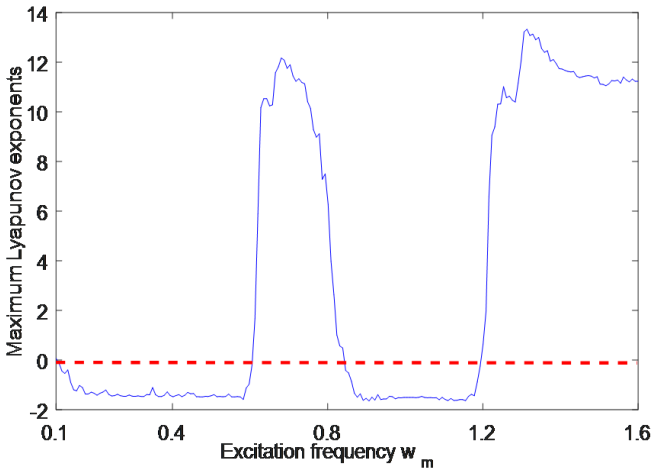


**Figure 14.** Lyapunov diagram of gear-bearing system with various excitation frequency $w_m$.

Furthermore, considering the strong nonlinearity, the time-domain chart, phase diagram, and Poincare section of the gear-bearing system corresponding to **Figure 13b** are depicted, as shown in **Figures 15–17**. It can be clearly observed that the gear-bearing system varies from the quasi-periodic to chaotic. **Figure 15** illustrates that while the value of excitation frequency is $w_m = 1.0$, the time-domain chart presents a sine or cosine curve, and the phase diagram is an ellipse which corresponds to a point in the Poincare section. The dynamic behavior reveals that the gear-bearing system is in a periodic motion. Depicted in **Figure 16** for $w_m = 1.4$ illustrates that the time-domain chart presents a periodic curve, and the phase diagram presents two multi-layered ellipses which correspond to two piles of points in the Poincare section. This phenomenon indicates the chaotic state of the gear-bearing system. Similarly, for the case of $w_m = 1.4$ in **Figure 17**, the time-domain chart presents a periodic curve. The phase diagram presents a multi-layered ellipse which corresponds to multiple discrete points in the Poincaré section, indicating that the gear-bearing system is in a chaotic state. The above dynamic behaviors manifest that the gear-bearing system exhibits more complicated motion with the excitation frequency increase.

## 5.2. Dynamic response influenced by fractal dimension

Fractal dimension is a key parameter leading to the enlargement of vibration and noise in gear-bearing systems. In order to investigate the influence of fractal dimension on dynamic response, **Figures 18–20** present the time-domain chart, phase diagram, frequency spectrum, and Poincare map with respect to various values of fractal dimension $D = 1.2$, $D = 1.5$ and $D = 1.9$ for the case of excitation frequency $w_m = 0.7$. We can observe from **Figures 18–20** that with the fractal dimension $D$ increasing from 1.2 to 1.5 and then 1.9, the magnitudes of the amplitude of the time-domain chart continuously

increase from 1.135 to 1.183 and then 1.187. Similar to the phenomenon of time-domain chart, the values of the frequency spectrum continuously increase from 0.2181 to 0.2292 and then 0.2316. Additionally, the phase diagram becomes gradually wider from a thin ellipse to a thick ellipse. And the Poincare map exhibits a more disordered point distribution.

The above phenomenon illustrates that with the fractal dimension increase, the dynamic response of the gear-bearing system is enlarged intuitively. Actually, in this particular case, the dynamic response is primarily affected by TVMS, which is sensitive to the fractal dimension, as demonstrated and elaborated in **Figure 9** in Subsection 2.3.

In summary, we can conclude that the fractal dimension can significantly affect the dynamic response of the gear-bearing system. In other words, the fractal dimension is an extremely critical parameter for improving the dynamic performance and minimizing vibration and noise of gear-bearing systems.

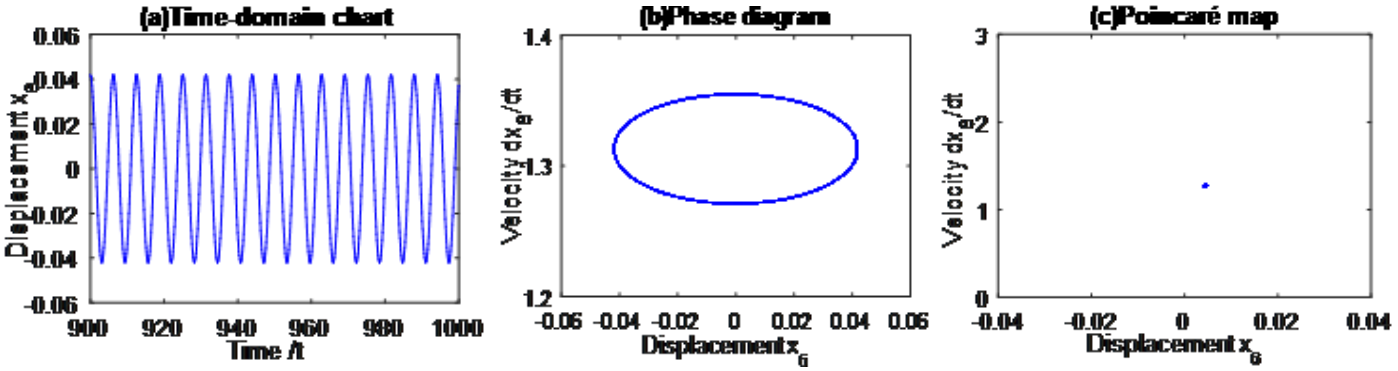


**Figure 15.** The dynamic response curves corresponding to excitation frequency $w_m = 1.0$.

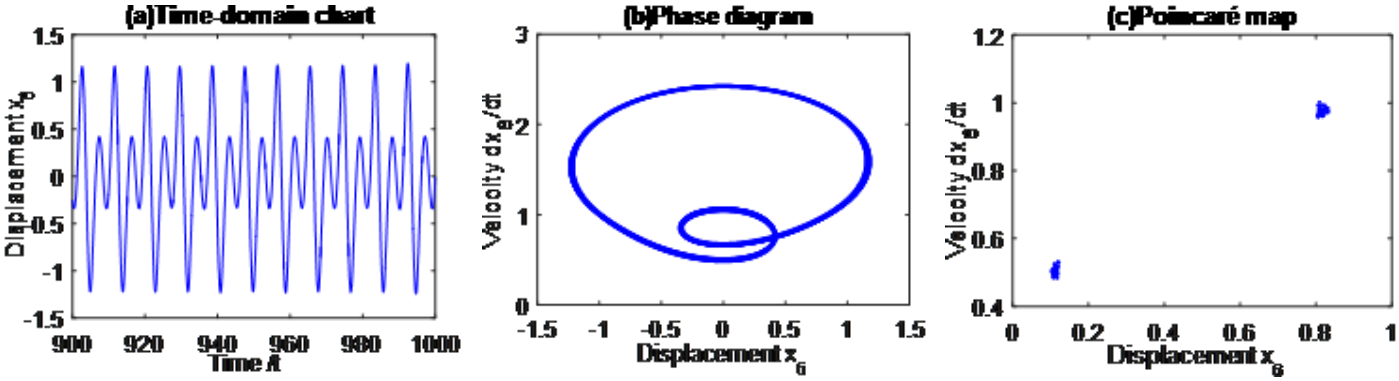


**Figure 16.** The dynamic response curves corresponding to excitation frequency $w_m = 1.4$.

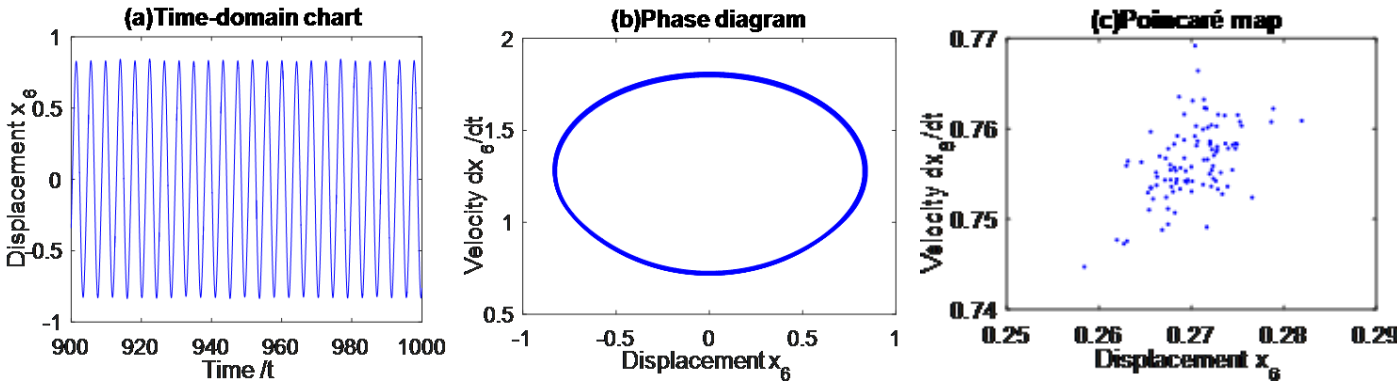


**Figure 17.** The dynamic response curves corresponding to excitation frequency $w_m = 1.5$.

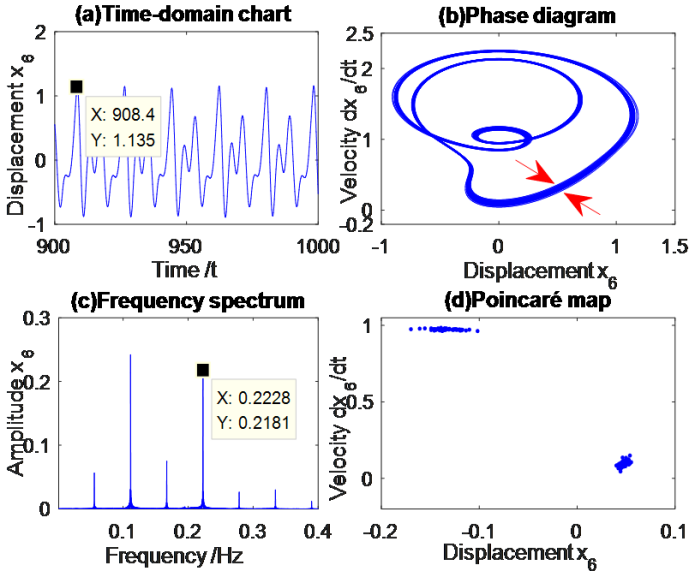


**Figure 18.** Dynamic response curves corresponding to fractal dimension $D = 1.2$.

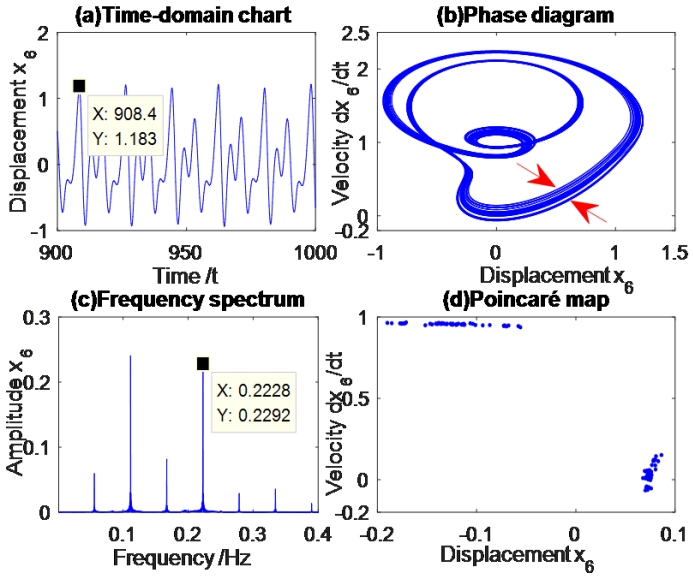


**Figure 19.** Dynamic response curves corresponding to fractal dimension $D = 1.5$.

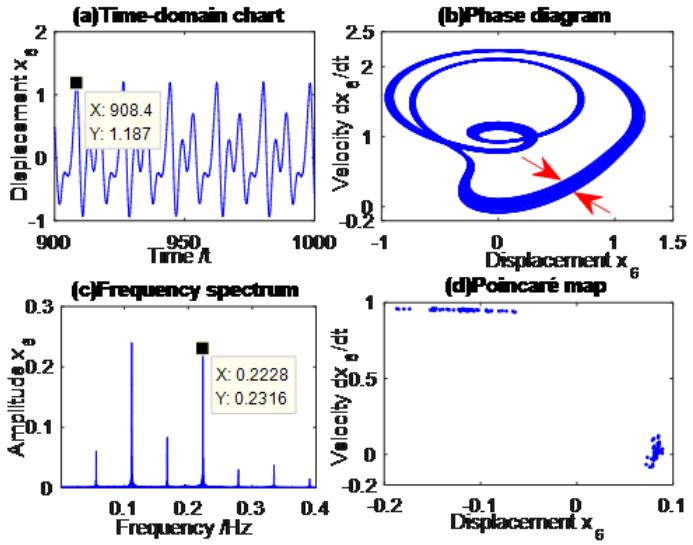


**Figure 20.** Dynamic response curves corresponding to fractal dimension $D = 1.9$.

### 5.3. Dynamic response influenced by fractal friction excitation

To further investigate the influence of fractal sliding friction, the bifurcation and chaos of the gear-bearing system with and without friction coefficient are compared theoretically. The bifurcation diagram of the gear-bearing system with various excitation frequency $w_m$ with respect to the friction coefficient $\mu = 0$ and $\mu = 0.04$ are presented figuratively, as depicted in **Figure 21**. It can be observed that, compared with the case of not considering the friction coefficient in **Figure 21a**, the displacement amplitude of the bifurcation diagram in **Figure 21b** are enlarged noticeably. Simultaneously, the corresponding chaotic state becomes more significant. These variations have been confirmed and marked with a red ellipse and a green ellipse. Additionally, the maximum Lyapunov exponent is carried out to evaluate the periodic motion and chaotic state illustrated in **Figure 22**. The Lyapunov diagram with respect to various excitation frequency $w_m$ corresponds to two main chaotic regions, which have been examined and demonstrated in the bifurcation diagram.

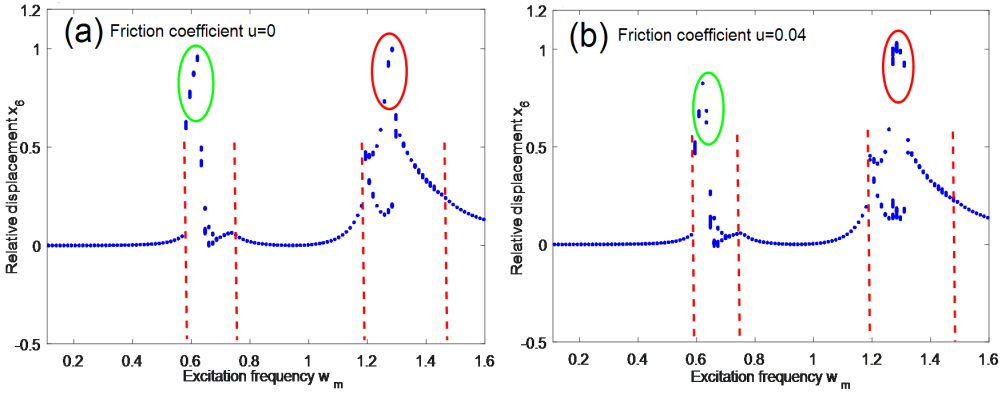


**Figure 21.** Bifurcation diagrams of gear system with various excitation frequency $w_m$ with respect to friction coefficient: **(a)** $\mu = 0$; **(b)** $\mu = 0.04$.

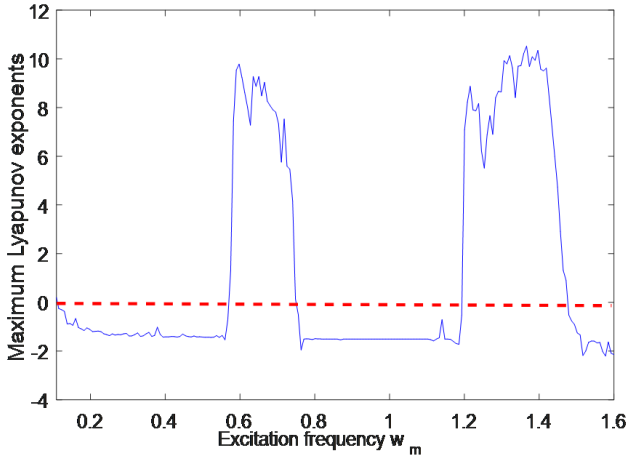


**Figure 22.** Lyapunov diagram of gear system with various excitation frequency $w_m$.

In addition to the comparison of bifurcation characteristics, the dynamic response of the gear-bearing system corresponding to excitation frequency $w_m = 0.65$ and $D = 1.2$ with respect to friction coefficient $\mu = 0$ and $\mu = 0.04$ is also compared directly, as depicted in **Figures 23** and **24**. It can be found that, compared with not considering friction in **Figure 23**, the displacement of the time-domain chart increases evidently after introducing the friction factor. The phase diagram becomes denser, and

the Poincare map exhibits a more disordered point distribution. On this basis, we also investigate the dynamic response corresponding to excitation frequency $w_m = 0.65$ and $D = 1.2$ with respect to the friction coefficient $\mu = 0$ and $\mu = 0.04$. Similar phenomena and conclusions can be discovered in **Figures 25** and **26**.

In our previous manuscript, we concluded that sliding friction is a key parameter and can affect the modal properties of the gear-bearing system [28]. In this analysis, we can also conclude that the bifurcation characteristic and dynamic response of the gear-bearing system are sensitive to the sliding friction.

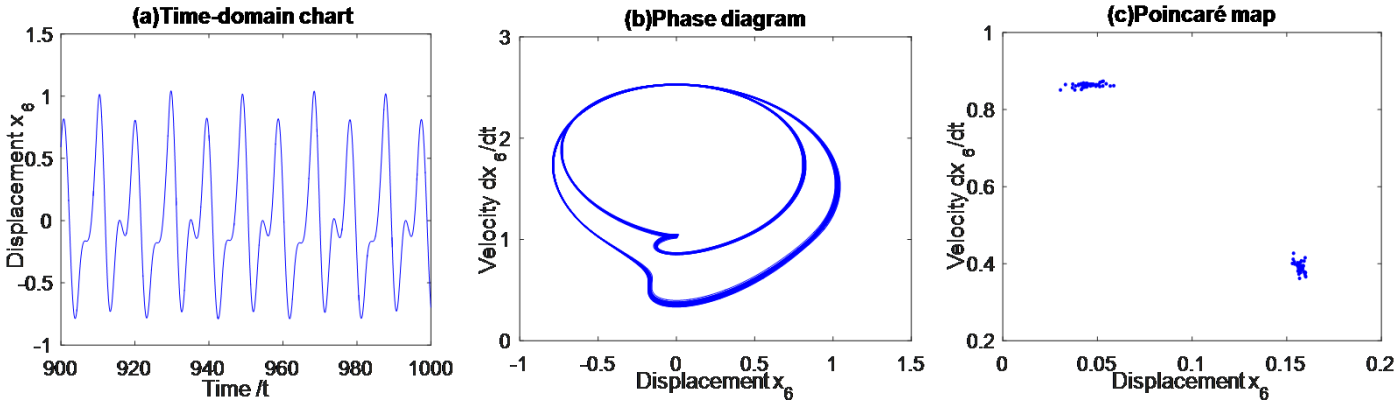


**Figure 23.** Dynamic response curves corresponding to excitation frequency $w_m = 0.65$, $D = 1.2$ and $\mu = 0$.

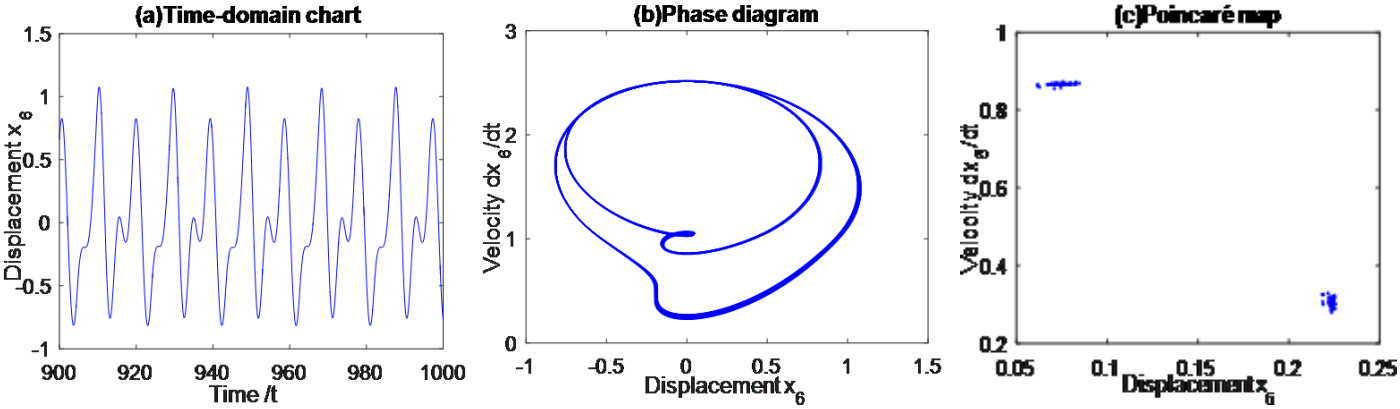


**Figure 24.** Dynamic response curves corresponding to excitation frequency $w_m = 0.65$, $D = 1.2$ and $\mu = 0.04$.

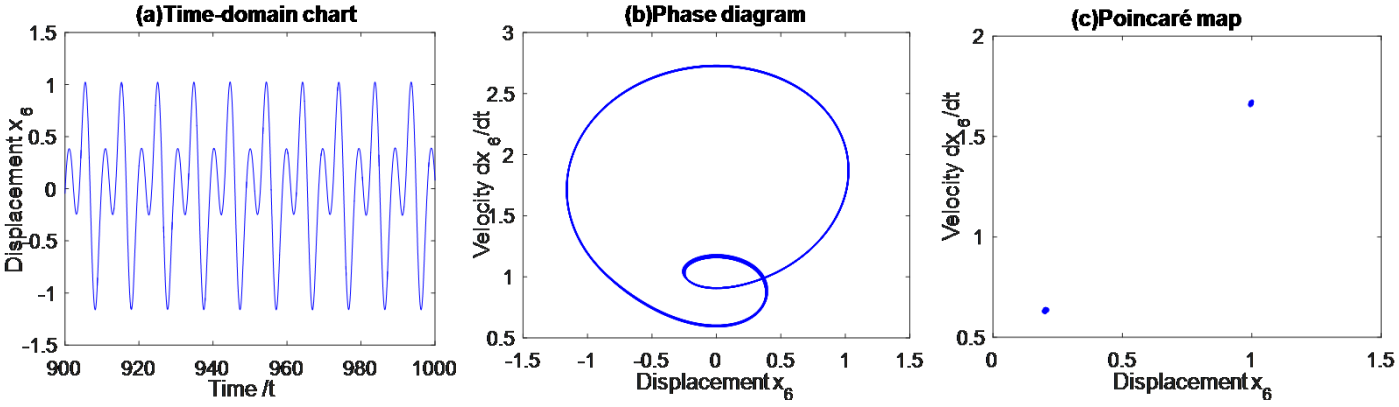


**Figure 25.** Dynamic response curves corresponding to excitation frequency $w_m = 1.284$, $D = 1.2$ and $\mu = 0$.

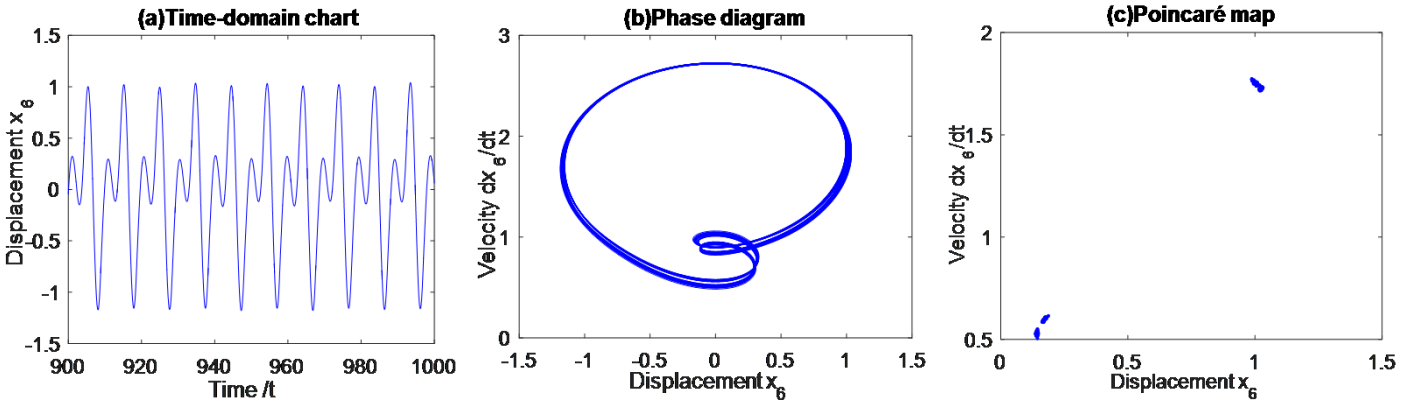


**Figure 26.** Dynamic response curves corresponding to excitation frequency $w_m = 1.284$, $D = 1.2$ and $\mu = 0.04$.

In summary, the sliding friction can significantly affect the nonlinear dynamics of the gear-bearing system, which is consistent with our previous conclusion in Wang and Zhu [30].

## 6. Conclusion

This work theoretically introduces fractal theory to evaluate the TVMS and nonlinear dynamics of gear-bearing system. The bifurcation characteristics with the case of considering and not considering fractal dimension and sliding friction are examined. The maximum Lyapunov exponent forecasting methodology is carried out to validate the dynamic characteristics. Ultimately, the nonlinear dynamic behaviors of the gear-bearing system are further investigated with the help of time-domain charts, frequency spectra, phase diagrams, and Poincare maps. The following conclusions can be drawn:

(1) The results show that after the introduction of fractal characterization, an irregular minor fluctuation was applied to the TVMS curve, which leads to the overall decrease of amplitude of meshing stiffness. With the fractal dimension increase, the minor fluctuation tends to decrease evidently.

(2) In comparison with not introducing fractal dimension case, the newly emerging chaotic motion of gear-bearing system considering fractal dimension is greatly weakened, which is primarily caused by the fluctuated meshing stiffness.

(3) The results also show that the bifurcation characteristic and dynamic response of the gear-bearing system are sensitive to the sliding friction, which makes the gear's vibration characteristics more complicated.

In summary, this work indicates that the fractal dimension and sliding friction have significant influence on the nonlinear dynamics of the gear-bearing system. This work is helpful for guiding gear surface design and improving the gear dynamic performance.

**Author contributions:** Conceptualization, WL, YC and QW; methodology, WL and YC.; validation, YC; investigation, QW; data curation, WL; writing—review & editing, WL and YC; writing—original draft preparation, WL and YC; visualization, WL; supervision, QW. All authors have read and agreed to the published version of the manuscript.

**Funding:** This work was funded by the Fundamental Research Funds for the Provincial Undergraduate Universities of Heilongjiang Province (Grant No. 2025-KYYWF-ZR0499), Natural Science Foundation of Heilongjiang Province (Grant No. PL2024E029) and Longjiang Project Young Goose Innovation Team Support Program (Grant No. 2024CYLJ02).

**Institutional review board statement:** Not applicable.

**Informed consent statement:** Not applicable.

**Data availability statement:** The authors do not have permission to share the data.

**Conflict of interest:** The authors declare that they have no known competing financial interests or personal relationships that could have appeared to influence the work reported in this manuscript.

**AI use statement:** The authors declare that no artificial intelligence (AI) tools were used in the preparation of this manuscript.

## References

1. Yao Z, Zhang S, Wu Z. Dynamic modeling and analysis based on torque signal of planetary gear system for tooth fault detection. Journal of Sound and Vibration. 2026; 634: 119784. doi: 10.1016/j.jsv.2026.119784
2. Liu Y, Wang J, Dong C, et al. A novel method for analyzing the dynamic wear characteristics of planetary gear train for non-circular gear hydraulic motor. Flow Measurement and Instrumentation. 2026; 110: 103305. doi: 10.1016/j.flowmeasinst.2026.103305
3. Rico-Vicente R, Díaz I, Justo X, et al. Comparative analysis of harmonic drive and planetary gear actuation units for exoskeletons using load cell-based transparency control. Mechatronics. 2026; 116: 103471. doi: 10.1016/j.mechatronics.2026.103471
4. Zhao H, Zang L, Zhen D, et al. Numerical calculation and experimental study of the influence of solid lubrication coating on the contact stiffness of planetary gears. Results in Engineering. 2025; 28: 108350. doi: 10.1016/j.rineng.2025.108350
5. Sciarra G, Mottola G, Casamenti G, et al. Omni: A low-backlash planetary Wolfrom gearbox with beveloid gears for robotic applications. Mechanism and Machine Theory. 2025; 214: 106098. doi: 10.1016/j.mechmachtheory.2025.106098
6. Sanchez-Espiga J, Fuerst M, Fernandez-del-Rincon A, et al. On the behaviour of n-planets planetary gear sets influenced by geometrical design factors. Mechanism and Machine Theory. 2025; 205: 105860. doi: 10.1016/j.mechmachtheory.2024.105860
7. Huang K, Cheng Z, Xiong Y, et al. Bifurcation and chaos analysis of a spur gear pair system with fractal gear backlash. Chaos, Solitons & Fractals. 2021; 142: 110387. doi: 10.1016/j.chaos.2020.110387
8. Wang L, Du Y, Bai H, et al. Research on nonlinear characteristics of multi-clearance gear system based on fractal theory. International Journal of Non-Linear Mechanics. 2025; 170: 104995. doi: 10.1016/j.ijnonlinmec.2024.104995
9. Chen Q, Ma Y, Huang S, et al. Research on gears' dynamic performance influenced by gear backlash based on fractal theory. Applied Surface Science. 2014; 313: 325–332. doi: 10.1016/j.apsusc.2014.05.210
10. Huang K, Xiong Y, Wang T, et al. Research on the dynamic response of high-contact-ratio spur gears influenced by surface roughness under EHL condition. Applied Surface Science. 2017; 392: 8–18. doi: 10.1016/j.apsusc.2016.09.009
11. Majumdar A, Bhushan B. Fractal Model of Elastic-Plastic Contact Between Rough Surfaces. Journal of Tribology. 1991; 113(1): 1–11. doi: 10.1115/1.2920588
12. Chen Q, Zhou J, Khushnood A, et al. Modelling and nonlinear dynamic behavior of a geared rotor-bearing system using tooth surface microscopic features based on fractal theory. AIP Advances. 2019; 9(1): 015201. doi: 10.1063/1.5055907
13. Han J, Li G, Tian X, et al. Nonlinear Dynamics Analysis of Gear Transmission System Based on Tooth Surface Microtopography. Journal of Vibration Engineering & Technologies. 2024; 12(2): 1753–1772. doi: 10.1007/s42417-023-00940-6

14. Mo G, Liu C, Liu G, et al. Improved Nonlinear Dynamic Model of Helical Gears Considering Frictional Excitation and Fractal Effects in Backlash. Machines. 2025; 13(4): 262. doi: 10.3390/machines13040262
15. Yu X, Sun Y, Li H, et al. Nonlinear characteristics of gear pair considering fractal surface dynamic contact as internal excitation. International Journal of Non-Linear Mechanics. 2022; 143: 104027. doi: 10.1016/j.ijnonlinmec.2022.104027
16. Wu S, Zhou Y, Xing W, et al. Research on the Contact Dynamic Characteristics of Gears Coupled with Tooth Surface Micromorphology and Spalling Faults. Journal of Vibration Engineering & Technologies. 2025; 13(5): 314. doi: 10.1007/s42417-025-01885-8
17. Xiong Y, Zhou Z, Huang K, et al. An improved fractal model for tangential contact damping of high contact ratio gear considering friction effect. Chaos, Solitons & Fractals. 2021; 153: 111510. doi: 10.1016/j.chaos.2021.111510
18. Zhu G, Huang K, Xiong Y, et al. An improved model for time-varying mesh stiffness of super-high-contact-ratio helical gear pair considering contact disparities on differently sliced fractal surfaces. Communications in Nonlinear Science and Numerical Simulation. 2025; 146: 108806. doi: 10.1016/j.cnsns.2025.108806
19. Sun X, Xin X. Fractal model of thermal contact conductance of the involute arc cylindrical gear considering friction coefficient. COMPEL—The international journal for computation and mathematics in electrical and electronic engineering. 2024; 43(1): 137–148. doi: 10.1108/COMPEL-07-2023-0317
20. Guo J, Dong C, Wei S, et al. New method for strength analysis of involute beveloid gears using fractal theory. Journal of Mechanical Science and Technology. 2024; 38(9): 4815–4825. doi: 10.1007/s12206-024-0817-2
21. Xu T, Wu S, Zhu W, et al. Influences of fractal characteristics of microscopic morphology of the meshing surface in a planetary gear train on the thermal mixed lubrication performance. Proceedings of the Institution of Mechanical Engineers, Part C: Journal of Mechanical Engineering Science. 2026; 240(7): 2404–2422. doi: 10.1177/09544062251409882
22. Cai ZJ, Zheng XQ, Lan H-Q, et al. Time-Varying Meshing Stiffness and Dynamic Parameter Model of Spiral Bevel Gears with Different Surface Roughness. Applied Sciences. 2024; 14(4): 1533. doi: 10.3390/app14041533
23. Siyu C, Jinyuan T, Caiwang L, et al. Nonlinear dynamic characteristics of geared rotor bearing systems with dynamic backlash and friction. Mechanism and Machine Theory. 2011; 46(4): 466–478. doi: 10.1016/j.mechmachtheory.2010.11.016
24. Howard I, Jia S, Wang J. The Dynamic Modelling of a Spur Gear in Mesh Including Friction and a Crack. Mechanical Systems and Signal Processing. 2001; 15(5): 831–853. doi: 10.1006/mssp.2001.1414
25. Saxena A, Parey A, Chouksey M. Time varying mesh stiffness calculation of spur gear pair considering sliding friction and spalling defects. Engineering Failure Analysis. 2016; 70: 200–211. doi: 10.1016/j.engfailanal.2016.09.003
26. Liu N, Ma H, Ding X, et al. Dynamic characteristics of rigid-flexible coupled planetary gear-bearing-rotor system considering the tooth surface lubrication friction and roughness. Mechanism and Machine Theory. 2025; 217: 106259. doi: 10.1016/j.mechmachtheory.2025.106259
27. Wang J, Zheng J, Yang A. An Analytical Study of Bifurcation and Chaos in a Spur Gear Pair with Sliding Friction. Procedia Engineering. 2012; 31: 563–570. doi: 10.1016/j.proeng.2012.01.1068
28. He S, Gunda R, Singh R. Inclusion of Sliding Friction in Contact Dynamics Model for Helical Gears. Journal of Mechanical Design. 2007; 129(1): 48–57. doi: 10.1115/1.2359474
29. Zhang K, Shen R, Hu Z, et al. Dynamic modeling and analysis considering friction-wear coupling of gear system. International Journal of Mechanical Sciences. 2024; 275: 109343. doi: 10.1016/j.ijmecsci.2024.109343
30. Wang S, Zhu R. Nonlinear dynamic analysis of GTF gearbox under friction excitation with vibration characteristics recognition and control in frequency domain. Mechanical Systems and Signal Processing. 2021; 151: 107373. doi: 10.1016/j.ymssp.2020.107373
31. Liang X, Zuo MJ, Patel TH. Evaluating the time-varying mesh stiffness of a planetary gear set using the potential energy method. Proceedings of the Institution of Mechanical Engineers, Part C: Journal of Mechanical Engineering Science. 2014; 228(3): 535–547. doi: 10.1177/0954406213486734
32. Liu N, Ma H, Guan H, et al. Analysis of meshing characteristics of planetary gear system considering tooth surface roughness and elastohydrodynamic lubrication. Journal of Central South University. 2025; 32(7): 2511–2534. doi: 10.1007/s11771-025-6020-5
33. Zheng J, Qin D, Liu C, et al. Improved Analytical Model for Mesh Stiffness of Helical Gears Considering the Relationship of Friction and Flash Temperature Under Steady Temperature Field. Journal of Tribology. 2025; 147(7): 071703. doi: 10.1115/1.4067812
34. Xiao H, Zhang F, Li Z, et al. Gear tribological and contact fatigue prediction with rough topography and groove texture under elastohydrodynamic lubrication. Meccanica. 2025; 60(9): 2641–2669. doi: 10.1007/s11012-025-02019-w

35. Li S, Kahraman A. Prediction of Spur Gear Mechanical Power Losses Using a Transient Elastohydrodynamic Lubrication Model. Tribology Transactions. 2010; 53(4): 554–563. doi: 10.1080/10402000903502279
36. Luo W, Qiao B, Shen Z, et al. Time-varying mesh stiffness calculation of a planetary gear set with the spalling defect under sliding friction. Meccanica. 2020; 55(1): 245–260. doi: 10.1007/s11012-019-01115-y
37. Liu W, Shuai Z, Guo Y, et al. Modal properties of a two-stage planetary gear system with sliding friction and elastic continuum ring gear. Mechanism and Machine Theory. 2019; 135: 251–270. doi: 10.1016/j.mechmachtheory.2019.01.026
38. Wei L, Kai S, Hailong S, et al. Modulation sideband analysis of a two-stage planetary gear system with an elastic continuum ring gear. Journal of Sound and Vibration. 2022; 527: 116874. doi: 10.1016/j.jsv.2022.116874
39. Liu W, Shi K, Tupolev V, et al. Nonlinear dynamics of a two-stage planetary gear system with sliding friction and elastic continuum ring gear. Journal of Mechanical Science and Technology. 2022; 36(1): 77–85. doi: 10.1007/s12206-021-1206-8
40. Bu H, Li J, Guo J, et al. Establishment of theoretical model and dynamic analysis of gear meshing force for the multi-gear driving system considering the effect of friction. Engineering Failure Analysis. 2025; 171: 109382. doi: 10.1016/j.engfailanal.2025.109382
41. Meng D, Yang H, Fazeres-Ferradosa T, et al. Time-varying mesh stiffness modelling of offshore wind gearboxes under multi-fault modes. Maritime Engineering. 2025; 178(4): 170–195. doi: 10.1680/jmaen.25.00031
42. Meng D, Nie P, Yang S, et al. Reliability analysis of wind turbine gearboxes: past, progress and future prospects. International Journal of Structural Integrity. 2025; 16(1): 4–38. doi: 10.1108/IJSI-08-2024-0129
43. Meng D, Wang H, Yang S, et al. Fault Analysis of Wind Power Rolling Bearing Based on EMD Feature Extraction. Computer Modeling in Engineering & Sciences. 2022; 130(1): 543–558. doi: 10.32604/cmes.2022.018123